Lab on a Chip

IMMUNOMAGNETIC LEUKOCYTE DIFFERENTIAL IN WHOLE BLOOD ON AN ELECTRONIC MICRODEVICE

Journal:	*Lab on a Chip*
Manuscript ID	LC-ART-02-2022-000137.R1
Article Type:	Paper
Date Submitted by the Author:	04-May-2022
Complete List of Authors:	Civelekoglu, Ozgun; Georgia Institute of Technology, Electrical and Computer Engineering Ozkaya-Ahmadov, Tevhide; Georgia Institute of Technology, Electrical and Computer Engineering Arifuzzman, A K M; Georgia Institute of Technology Islak Mutcali, Sibel; Emory University, Winship Cancer Institute Sarioglu, A.; Georgia Institute of Technology, Electrical and Computer Engineering

IMMUNOMAGNETIC LEUKOCYTE DIFFERENTIAL IN WHOLE BLOOD ON AN ELECTRONIC MICRODEVICE

Ozgun Civelekoglu [a], Tevhide Ozkaya-Ahmadov [a], A K M Arifuzzman [a], Sibel Islak Mutcali [b], A. Fatih Sarioglu [a,c,d]

[a] School of Electrical and Computer Engineering, Georgia Institute of Technology, Atlanta, Georgia 30332, USA
[b] Winship Cancer Institute, Emory University, Atlanta, Georgia 30322, USA
[c] Parker H. Petit Institute for Bioengineering and Bioscience, Georgia Institute of Technology, Atlanta, Georgia 30332, USA
[d] Institute for Electronics and Nanotechnology, Georgia Institute of Technology, Atlanta, Georgia 30332, USA
[*] Correspondence should be addressed to A.F.S. (sarioglu@gatech.edu)

ABSTRACT

Leukocytes are the frontline defense mechanism of the immune system. Their composition dynamically changes as a response to a foreign body, infection, inflammation, or other malignant behavior occurring within the body. Monitoring the composition of leukocytes, namely leukocyte differential, is a crucial assay periodically performed to diagnose an infection or to assess a person's vulnerability for a health anomaly. Currently, leukocyte differential analysis is performed using hematology analyzers or flow cytometers, both of which are bulky instruments that require trained and certified personnel for operation. In this work, we demonstrate a new technique to obtain leukocyte differentials in a highly portable and integrated microfluidic chip by magnetically analyzing the CD33 expression of leukocytes. When benchmarked against conventional laboratory instruments, our technology demonstrated < 5% difference on average for all subtypes. Our results show that hematology testing could be performed beyond the centralized laboratories at a low cost and ultimately provide point-of-care and at-home testing opportunities.

INTRODUCTION

Leukocytes, also known as white blood cells (WBCs), are the hematological cells involved in the immune response of a body. Each leukocyte subtype, namely lymphocytes, granulocytes, and monocytes, carries out a specific task in the immune system. Lymphocytes are involved in recognizing foreign bodies and producing antibodies as a defense mechanism (1, 2). Granulocytes respond to bacterial or fungal infections, allergic reactions, and inflammations (3). Monocytes are engaged in endocytotic activities (4, 5). These cells can be differentiated from each other based on their biophysical and biochemical properties, such as their antigen expression, mono-/multi-nuclear composition and size.

Measuring proportions of leukocyte subtypes in blood, which is called a differential, is a routine assay performed in clinics to find blood disorders, potential infections, or specific vulnerabilities. For example, neutropenia, which is the deficiency of neutrophils (a subtype of granulocytes), is a condition that leaves the body heavily predisposed to infections (6) and must be kept under observation while the patient is taking broad spectrum antibiotics (7). Similarly, CD4+

lymphocytopenia (or lymphopenia, i.e., deficiency of CD4+ lymphocytes) is observed in infections and autoimmune diseases such as AIDS (8-10). Beyond deficiencies, diseases and disorders may also present themselves as unnatural abundance of cells, such as monocytosis (11) which is often caused by tuberculosis (12, 13), subacute bacterial endocarditis (14) or malaria (15). The prognosis of these diseases relies on periodic leukocyte differentials (16-18). For example, neutropenia patients get tested for their leukocyte differentials at least 3 times a week for a duration of 6 weeks (16).

Conventionally, the leukocyte differentials are measured via hematology analyzers (19), which are also known as complete blood count (CBC) analyzers. To analyze the leukocytes, these instruments lyse the erythrocytes and measure the impedance of cells. Based on the impedance of the cells and the device-specific parameters, the leukocytes are categorized into lymphocytes, granulocytes, and monocytes. Leukocyte differentials are also measured by flow cytometry in clinical research (20, 21) by investigating fluorescently labeled leukocytes under laser exposure. Both approaches require bulky instruments and certified technicians for operation often in a centralized laboratory, inducing a limited access in resource-poor regions.

Recently, alternative methods have been developed to address the limitations of the existing instrumentation by using machine learning for classification from cell images (22), using refractive index tomography (23), Raman spectroscopy (24), miniaturized laser setups with fluorescent dyes (25-28) or low-cost systems such as smartphone-coupled paper-based assays (29, 30) and microfluidic platforms with impedance measurements (31-33) and capture arrays (34, 35). However, these works were often unable to process the samples with erythrocytes present due to the overwhelming interference they would cause. Hence, these works resorted to preliminary sample preparation protocols such as cell lysis or filtration.

We recently developed an integrated microfluidic chip that can profile cell surface antigens directly from whole blood samples using immunomagnetic sorting [36, 37] as a point-of-care-suitable form of flow cytometry (38-40). In this work, we apply our technology to develop an electronic leukocyte differential assay that can directly analyze whole blood samples on a low-cost and portable microfluidic chip. Briefly, our assay first separates immunomagnetically labeled leukocytes from other blood cells and later differentially sorts them based on their immunomagnetic load to fractionate those leukocytes into subsets. As the results are readily available as an electrical signal, the presented platform is ideal for expanding the leukocyte differential analysis to virtually any setting, point-of-care, bedside, or home, for effortless and rapid monitoring of immunological disorders and emergencies. Hence it offers the potential to eliminate periodic hospital visits that are particularly risky for patients with immunodeficiencies.

MATERIALS AND METHODS

Microchip design and operation. To profile the leukocyte subpopulations in a blood sample, we targeted the membrane protein CD33, whose expression is known to vary among the leukocyte subpopulations (41). More specifically, monocytes express the highest level of CD33, while granulocytes have a medium and lymphocytes have the lowest expression (Supplementary Figure 1). To profile the CD33 expression of leukocytes, we utilize cascaded magnetophoretic sorters and perform sample purification and cell characterization all within a single microfluidic chip. Since the magnetic load on a leukocyte corresponds to the density of the target surface

antigen (42, 43), discriminating or gating leukocytes based on the number of magnetic beads they carry is equivalent to the widely adopted strategy of gating cell populations based on the fluorescent intensity in a conventional flow cytometer.

Our magnetophoretic cytometer (MACY) involves four stages (Figure 1a): First, we label the leukocytes with anti-CD33 conjugated magnetic microbeads. Second, we perform a binary separation utilizing the immunomagnetic load on the leukocytes unlike the rest of the blood cells. Third, the purified sample proceeds to a characterization stage where the leukocytes are differentially sorted according to their surface expression. Finally, we quantify the separated subset fractions with a network of barcoded electrical sensors.

Our microfluidic chip is composed of microfluidic channels molded in polydimethylsiloxane (PDMS) to manipulate the sample flow and gold electronic sensors patterned on a glass substrate for cell characterization (Figure 1b). The PDMS mold was fabricated by patterning 25 μm-thick SU-8 negative photoresist (SU-8 2025, MicroChem) on a 4-inch silicon wafer using a maskless aligner (MLA1500, Heidelberg). Prior to its first use, the mold was treated with trichloro(octyl)silane overnight for effortless peel-off. The polymer and its crosslinker (Sylgard 184, Dow Corning) were mixed at 10:1 ratio by weight, and the mixture was poured onto the mold. After degassing, the PDMS was cured in an oven at 65℃ for 8 hours, and finally peeled off from its mold. The electrode design was patterned on a 2-inch by 3-inch glass slide by photolithography using NR9-1500PY photoresist (Futurrex). A 500 nm-thick film of chrome/gold layer was then deposited on the glass slide using an e-beam evaporator (Denton Explorer), and the sacrificial layer was lifted off in an acetone bath under mild sonication. Finally, the PDMS layer and the glass substrate were permanently bonded after an oxygen plasma treatment. To ensure proper alignment of each component, we designed a 3D-printed assembly that also accommodates four neodymium magnets to supply magnetic gradient for cell manipulation. The combined cost of the materials and the microfabrication of the chip as a research-grade prototype was estimated to be ~4 USD per chip, which is expected to be an order of magnitude lower when mass-manufactured.

Upon the introduction of the sample (at 1.5 mL/h) and 1X phosphate buffered saline (at 4.9 mL/h), immunomagnetically-labeled cells in the sample were first pulled to the central buffer stream under the magnetic field gradient for subsequent analysis (Figure 1c). The leftover sample, mostly made up of erythrocytes then continue to a second pass to achieve a higher purification efficiency by capturing any residual leukocytes before being discarded from the chip.

To quantify the cells and capture the specific information of each cell, we used the code-multiplexed Coulter sensors (44-46). We designed a total of 16 sensors to be distributed across the device with each one assigned a unique 31-bit digital code from a set of orthogonal Gold sequences (47). Due to the orthogonality of these codes, signals from individual sensors could be distinguished from one another through correlation with a template library. The codes were embedded into the sensor structure by the spatial arrangement of positive and negative electrode fingers around an excitation electrode that supplied power to the circuitry. The sensors transduced three parameters into the digital codes they produced when cell interacted with them (Figure 1d): The power of the code signal represented the cell's size, the duration of the signal

provided the cell's speed, and the code itself provided the position of the cell on the microfluidic device. The electrical output signal from the microfluidic device was sampled into a computer for decoding the data to recover information for individual cells.

Magnetic force calculations. To calculate the immunomagnetic load (i.e., antigen expression) from the raw data from our sensors, we developed a numerical model of the microfluidic sorter for finite element analysis. First, the magnetic field was simulated in 3-dimensional space with COMSOL Multiphysics 5.4. and the simulated field was then projected into 2-dimensional planes to be combined with the hydrodynamic field and particle flow. Specifically, we employed the Magnetic Fields, No Current (mfnc), Laminar Flow (spf) interfaces and the Particle Tracing Module to capture the cell dynamics under device operation.

Our simulations have predicted up to 2 pN magnetic pull force per bead in the central binary separator and from 0.85 to 1 pN force per bead in the secondary pass (Figure 2a). The differential sorting chambers were asymmetrically placed to increase the total dynamic range of the system, and consequently, the top sorter was predicted exerting up to 0.8 pN while the bottom sorter was estimated to exert up to 0.4 pN per bead. We then compiled a cumulative look-up table for the top and the bottom sorters by sweeping feasible combinations of cell size and surface expression (Figure 2b).

Donor recruitment and informed consent. Healthy adults volunteering to participate in this project were recruited according to a Georgia Tech Institutional Review Board (IRB) approved protocol. Each donor signed a written consent form before donating blood samples. All experiments were performed in compliance with the IRB-approved protocol, institute guidelines, local and federal law.

Sample collection and preparation. Venous blood samples were collected into K2-EDTA Vacutainers (i.e., lavender-top) from healthy volunteers in accordance with a protocol approved by Georgia Tech Institutional Review Board. Each blood sample was then separated into four aliquots for testing and three independent validation studies. To label leukocytes, biotin conjugated anti-CD33 antibody (Cat. no: 366628, BioLegend) was introduced into the testing aliquot at a concentration of 45 fg antibody per WBC and incubated for 30 minutes at room temperature. Then, 1 μm streptavidin conjugated magnetic beads (Cat. no: 65001, Invitrogen) were washed, pelleted, and added into the blood sample at a concentration of 100 beads per WBC. The mixture was incubated for 30 more minutes at room temperature in the absence of any magnetic field interference to ensure against aggregation of the beads. The assay uses commercially available reagents for the magnetic labeling, whose cost was calculated to be less than 0.30 USD per analysis of 10,000 leukocytes.

Preparation of granulocyte-rich blood samples. Blood samples from healthy donors were placed into SepMate (Cat. No: 85450, STEMCELL Technologies) isolation tubes that were supplemented with Lymphoprep (Cat. No: 07801, STEMCELL Technologies) density gradient medium. Granulocytes and erythrocytes were separated from the plasma and from the mononuclear cells via centrifugation at 1200g rpm for 10 minutes. The separation yielded three suspensions containing (1) granulocytes and erythrocytes, (2) lymphocytes and monocytes and (3) blood plasma. Granulocyte-erythrocyte suspension was mixed with the blood plasma at 1:1

ratio to dilute the dense cell population into proper hematocrit levels. Finally, the samples were aliquoted for testing and validation. For the test sample, the same immunomagnetic labeling protocol was followed.

Electrical signal acquisition and processing. The electrical sensors on the assay were driven through the excitation electrode of the sensor network with a $1.5V_{pk}$ 500 kHz sine wave. The sensing electrodes (2 positive and 2 negative) were first connected to transimpedance amplifiers to transduce the measured electrical current from the sensor to voltage signals (Supplementary Figure 2). These voltage signals were then sampled at 57.6kHz via a lock-in amplifier. The data stream was saved as a local file on the computer and were later processed by a MATLAB program that extracts the identity of the sensor (i.e., cell's location) as well as the cell velocity and cell size.

In processing the acquired electrical signal from the device, we first computed the correlation between the recorded signal and the previously created template library containing signals for each sensor on the device. The orthogonality of the code sequences produced by sensors ensured minimal crosstalk between different sensors and allowed identification of the matching sensor from an autocorrelation peak. For the cases where multiple cells interacted with different sensors simultaneously, an iterative successive interference cancellation algorithm was employed, and the interfering signals were subtracted until no residual signal remains in the waveform. Finally, immunomagnetic load on each of the sorted leukocytes was calculated by applying the computationally produced look-up table on the information gathered by the sensor built-in sensor network.

Flow cytometry analysis. After a sample was aliquoted for testing and validation, the validation sample was labeled with allophycocyanin (APC) conjugated anti-CD45 antibody (Cat. No: 368512, BioLegend) and phycoerythrin (PE) conjugated anti-CD33 antibody (Cat. No: 366608, BioLegend). After 30 minutes of incubation in dark, the erythrocytes were lysed using a lysis buffer (Cat. No: 420302. BioLegend). Upon 15 minutes of orbital shaking, the samples were analyzed with a BD LSRIIFortessa flow cytometer. Analysis of the flow cytometry data was performed in FlowJo (FlowJo, LLC).

RESULTS

Setting immunomagnetic load gates for leukocyte differential

To determine the quantitative gating parameters for discriminating the leukocytes based on their immunomagnetic load, we processed blood samples from different healthy donors and calibrated our data using leukocyte differential obtained from a commercial hematology analyzer using matched samples. Based on this calibration process, we set two immunomagnetic gates at 23 beads and 58 beads for our assay to differentiate leukocyte subpopulations. Next, to validate these set gates, we analyzed blood samples from three different healthy donors. Driving blood samples through our microfluidic chip at 1,500 μL/h, we recorded at least 4,000 events (to collect sufficient data points) in less than 5 minutes. First, we analyzed the density scatter graphs of the acquired data to identify the locations of the subpopulations (Figure 3a). In all cases, three distinct groups of cells clustered based on contrast in the cell size and immunomagnetic load could be identified qualitatively. Given lymphocytes were expected to have the least expression of CD33 among other leukocyte subpopulations, leukocytes with immunomagnetic load of < 23

beads were scores as lymphocytes. On the other end of spectrum, monocytes have the highest CD33 expression (Supplementary Figure 1) and larger in size (48) and accordingly leukocytes carrying >58 magnetic beads were scored as monocytes. Finally, the most populous fraction of leukocytes fell between the gates at 23 and 58 beads and these were labeled as granulocytes, consistent with the fact that on average CD33 expression of granulocytes falls between lymphocytes and monocytes.

Applying the set immunomagnetic load gates to our electrical cell sorting data, we then calculated the frequency of different leukocyte subpopulations for each donor (Figure 3b). We measured lymphocyte frequency to be 34.46%, 27.56% and 36.38% for Donors #1, #2 and #3, respectively. Likewise, we measured the granulocytes to be 54.32%, 63.24% and 55.32% and monocytes to be 10.22%, 9.22% and 8.30% of all leukocytes in the samples from Donors #1, #2 and #3, respectively. To test the accuracy of our measurements, we performed three independent analyses on the validation aliquots for each donor (Table 1). First, we fluorescently stained the sample against CD33 and analyzed the distributions using flow cytometry for a direct comparison to our CD33 measurements (Figure 3c). Fluorescence-based measurement of CD33 expression resulted in estimated concentrations of 34.2%, 29.3% and 35.3% for lymphocytes; 55.0%, 62.1% and 54.4% for granulocytes, and 10.8%, 8.6% and 10.3% for monocytes in samples from Donors #1, #2 and #3, respectively. Assuming the CD33-based flow cytometry results as the ground truth, the close match between the two assays confirmed the validity of our technology. Nevertheless, we also analyzed the sample with a standard hematology analyzer (Cell Dyn Emerald, Abbott) as well as with another set of flow cytometry measurements this time with CD45 stain and used the conventional side scatter versus CD45 expression method to quantify the fractions of different leukocyte subpopulations.

Benchmarking the assay against conventional methods

To quantitatively compare the results from our assay and the conventional methods, we computed the absolute percentile error in estimated subpopulation frequency (Figure 4a) and the relative percentile errors (Figure 4b). The absolute percentile error between the frequency measurements from MACY and the validation methods were consistently below ±2.5% on average for all leukocyte subtypes. In terms of the relative percentile error, when compared with the hematology analyzer results, our lymphocytes and granulocytes measurements had shown accurate results with an average relative percentile error of 3.8% (STD = 2.5) and 0.4% (STD = 1.69), respectively. Monocyte measurements, on the other hand, were consistently underestimated by our chip and showed a negative mean absolute percentile error (-1.3%) and much higher relative percentile error with a mean of -15.6% (STD = 8.28). This is because of the scarcity of monocytes among other leukocytes, which amplified even small differences in absolute frequency measurements when represented as relative percentile errors. On the other hand, when we compared our results to CD33-based flow cytometry, our calculations showed a uniform difference over all the subtypes. They also demonstrated lower means in relative percentile errors, but larger standard deviations with -0.73% (STD = 4.7), 0.76% (STD = 1.73) and -5.78% (STD = 13.4) for lymphocytes, granulocytes, and monocytes, respectively. The conventional flow cytometry method (side scatter vs CD45) also validated our findings with our device presenting -5.98% (STD = 2.74), 4.19% (STD = 2.19) and -5.71% (STD = 12.35) relative percent error. The larger standard deviation observed in comparing our assay results against the flow cytometry data was likely a result of the user-defined gating parameters which varied

between flow cytometry analyses. In contrast, hematology analyzers use fixed gating parameters defined during manufacturing regardless of the sample.

To test the consistency of our measurements with the conventional methods, we also used linear regression analysis. Specifically, we regressed subpopulation frequencies measured by our assay with respect to the same measurement performed by other techniques (Table 2). For granulocytes and lymphocytes, regression analysis showed a better fit (R^2>0.83), in particular with respect to CD45 flow cytometry measurements (R^2>0.92). Monocyte measurements were less accurate with R^2 values ranging between 0.56 to 0.74, matching best with CD45 flow cytometry data. In addition, our measurements with respect to the hematology analyzer resulted in a slope less than 1 and an intercept greater than 0 for all leukocyte populations, meaning we overestimated the fractions up to a point and underestimated beyond. We calculated these transition points to be 25%, 60% and 10% for lymphocytes, granulocytes, and monocytes, respectively. With respect to flow cytometry measurements of CD33 and CD45 expression, our regression analysis produced slopes close to 1 for lymphocytes and granulocytes, demonstrating the close agreement between those results and ours as discussed earlier and was also expected as our assay and flow cytometry employed the same parameter for leukocyte differentiation (i.e., membrane antigen expression).

Validation of the assay on samples with manipulated leukocyte compositions

To simulate hematological conditions with abnormal leukocyte compositions, we prepared blood samples with their mononucleated cells (i.e., lymphocytes and monocytes) depleted leading to abnormally high frequency of granulocytes among leukocytes (Materials and Methods). We analyzed these samples at 1,500 μL/h in our device and analyzed a minimum of 4,000 leukocytes for each run. In agreement with manipulated leukocyte composition, our assay reported abnormally high levels of granulocytes at 78.48%, 72.30% and 84.53% for Samples #1, #2 and #3, respectively (Figure 5a). We compared these measurements to the results from matched samples processed with a hematology analyzer (Cell Dyn Emerald, Abbott), as well as with CD33- and CD45-florescence flow cytometry. Our results were in close agreement with both the CD33-based (Figure 5b) and CD45-based flow cytometry data (Figure 5c). For the Sample #1, we measured the granulocyte frequency to be 78.48%, which closely agreed (<%3 difference) with the measurements of 81.1% from the CD33-based and 79.2% from the CD45-based flow cytometry. Similarly, our lymphocyte measurements differed with <2% deviation. For the Sample #1, the largest mismatch was observed with measured monocyte frequencies. Our measurement of 9.26% monocyte fraction was higher compared to both CD33-based and CD45-based flow cytometry at 5.3% and 5.73%, respectively. In Sample #2, although we captured the expected high levels of granulocytes for the, our granulocyte measurement of 72.30% fell short of measured concentrations of 79.3% and 82.5% for granulocytes from CD33 and CD45-based flow cytometry. The underestimation of granulocyte frequency then led to a considerable overestimation (25.54% versus 15.1% and 14.3% for CD33 and CD45) in the measured lymphocyte frequency. Finally, for Sample #3, our assay correctly identified the sample as the one with the highest frequency of granulocytes among tested samples with a measured granulocyte frequency of 84.53%. These measurements further validated the identity of the leukocytes that fell between our set immunomagnetic gates of 23 and 58 beads as granulocytes. Overall, our results agreed well with independent analyses. Larger deviations observed in some measurements are expected to result from the limited dynamic range of our assay in comparison

to fluorescence-based flow cytometry, which especially affects the analysis of samples, where surface expression levels between leukocyte subpopulations overlap considerably.

To further validate our immunomagnetic gates, we also processed the residual samples containing only the mononuclear cells and the blood plasma, which was readily available as byproducts from the preparation of granulocyte-rich blood samples (Materials and Methods). These samples were virtually absent of granulocytes as those were depleted along with the erythrocytes to prepare primary suspensions analyzed previously. Indeed, our assay detected abnormally low (~1.5%) levels of leukocytes with magnetic loads of 23-58 magnetic beads. Instead, we observed high fractions of either leukocytes carrying <23 magnetic beads (i.e., lymphocytes) or those that carried >58 magnetic beads (i.e., monocytes) in these samples (Supplementary Figure 3a) with a peak below 23 beads for lymphocytes and another peak beyond 58 beads for monocytes. Furthermore, those results were in good agreement with fluorescence-based flow cytometry of CD33 (Supplementary Figure 3b) and CD45 (Supplementary Figure 3c) expressions from these control samples. The hematology analyzer, on the other hand, was unable to provide any numerical output, but consistent error flags for these samples as they fell out of expected range. Taken together, these results validated the applicability of our immunomagnetic gates for discrimination of leukocytes based on CD33 expression.

Finally, to quantitively analyze the fit between results from our assay and the established leukocyte differential measurements, we compared the measured leukocyte compositions between different assay over all tested samples with manipulated leukocyte compositions. In these comparisons, when the absolute percentile errors for all subpopulations were considered, our measurements were on average within ±5% of the results from conventional methods used for validation (Figure 6a). On the other hand, the absolute percentile errors translated into larger differences when the relative percentile errors were considered within each population (Figure 6b). Specifically, because lymphocytes and monocytes were depleted in these test samples, relative errors were higher in those subpopulations. For example, an average absolute percentile error of ~4% (versus CD45-FC) in lymphocyte frequency led to an in-population relative percentile error of ~31%. Likewise, <1% mean absolute percentile error in monocyte frequency (versus CD45-FC), produced an average of ~15.5% in-population relative percentile error due small number of monocytes in the test sample. In contrast, the relative and absolute percentile errors were similar for leukocytes that were present in large numbers. For example, we observed a mean absolute percentile error as high as 4.9% (versus CD45-FC) for granulocytes, which translated into a mean relative percentile error of -4.03%.

DISCUSSION

We introduced an electronic microchip-based assay to perform 3-differential leukocyte analysis from peripheral whole blood by profiling the CD33 expression of leukocytes. The conventional methods, namely the hematology analyzers and flow cytometry, resort to the lysis of erythrocytes and/or sample dilution to examine the leukocytes and require at least a benchtop-scale instrument to perform the analysis. Our approach, on the other hand, accepts the whole blood sample mixed with magnetic microbeads directly. The embedded electrical sensors in the platform allow rapid cell characterization with a simple electronic circuit which can easily be constructed within a highly mobile, handheld device. Furthermore, the chips we used were

fabricated to be disposable ensuring against potential cross-contamination-induced measurement artifacts and eliminated the need for washing process required by a regular sample injection port between uses in leukocyte differential measurements.

In addition, our technology's utility for leukocyte differentials at the point-of-care or at home settings can be further enhanced by integrating the sample labeling process into our assay. As such, to streamline leukocyte labeling, blood can be collecting directly into a specialized vacutainer pre-deposited with antibody-conjugated magnetic beads. In this scenario, the sample preparation can be completed by mechanically agitating the collection tube – an act that can also be performed by a custom-built instrument in an automated fashion. In fact, some of the commercial hematology analyzers follow this system-level automation route by implementing traditional laboratory processes within a benchtop instrument to create sample-to-answer platforms. However, considering the simplicity of our sample preparation process with no need for wash or lysis steps, we could potentially achieve immunomagnetic labeling of leukocytes directly within the microfluidic device. One could use pre-deposit antibody-conjugated magnetic beads into device during manufacturing and employ active or passive microfluidic mixers to mix the sample with these beads as the leukocytes are driven through the device for analysis. Moreover, the whole operation can be automated using feedback-controlled magnetophoresis guided by artificial intelligence (49) to enable user-independent analysis. Such a system would truly enable a low-cost, self-administered at-home testing of leukocyte differentials at an increased frequency than otherwise possible in the clinics.

Finally, the platform leukocyte differential technology presented in this paper can be expanded to accommodate subjects that potentially present heterogeneity levels greater than observed in this work – a plausible scenario especially if subjects suffer from anomalies leading to drastic deviations from the expected levels of CD33 surface expression from leukocytes. To accommodate such cases, a potential strategy could be to combine different modalities for leukocyte differential with our device. Specifically, our assay inherently contains the size information for each processed leukocyte, as measured by the electrical sensor network once they are sorted by the microfluidic chamber. Given that commercially available 3-diff hematology analyzers solely rely on impedance-based electrical signals (i.e., cell size) for leukocyte differentials, we can potentially utilize this readily available information along with membrane protein expression on leukocytes for leukocyte differentials with greater accuracy and robustness against biological heterogeneity and noise.

CONCLUSION

Leukocytes are the frontline troops in our immune system, so their quantification and differentials carry vital information about our health. Our technology has the potential to make this available at point-of-care or bedside for identifying and managing immunological emergencies such as neutropenia, monocytosis or lymphocytopenia. With the wider adoption of telehealth services, devices that can process blood in a simple manner such as ours could further enhance the reach of healthcare by enabling various other home testing which would be followed by virtual consultations.

AUTHOR CONTRIBUTIONS

O.C., T.O.A and A.F.S designed the study. O.C. and A.K.M. performed the microfabrication in the cleanroom. O.C. performed the experiments. O.C., T.O.A, S.I.M and A.F.S. analyzed the data. O.C., T.O.A. and A.F.S. wrote the manuscript.

CONFLICT OF INTEREST

The authors declare no conflicting financial interests.

ACKNOWLEDGEMENTS

The work was sponsored by the National Science Foundations (NSF) through Award No: ECCS 1610995 and Award no: ECCS 1752170, and the Arnold and Mabel Beckman Foundation through Beckman Young Investigator Award to A.F.S. The authors would also like to thank Brandi E. Swain and Georgia Tech Stamps Health Services for their assistance in the collection of blood specimens.

REFERENCES

1. LeBien TW, Tedder TF. B lymphocytes: how they develop and function. Blood. 2008;112(5):1570-80.
2. Fabbri M, Smart C, Pardi R. T lymphocytes. The International Journal of Biochemistry & Cell Biology. 2003;35(7):1004-8.
3. Cannistra SA, Griffin JD. Regulation of the production and function of granulocytes and monocytes. Semin Hematol. 1988;25(3):173-88.
4. Cohn ZA. The Structure and Function of Monocytes and Macrophages. In: Dixon FJ, Kunkel HG, editors. Advances in Immunology. 9: Academic Press; 1968. p. 163-214.
5. Coillard A, Segura E. In vivo Differentiation of Human Monocytes. Frontiers in Immunology. 2019;10.
6. Boxer L, Dale DC. Neutropenia: Causes and consequences. Semin Hematol. 2002;39(2):75-81.
7. Hansen BA, Wendelbo O, Bruserud O, Hemsing AL, Mosevoll KA, Reikvam H. Febrile Neutropenia in Acute Leukemia. Epidemiology, Etiology, Pathophysiology and Treatment. Mediterr J Hematol Infect Dis. 2020;12(1):e2020009.
8. Pothlichet J, Rose T, Bugault F, Jeammet L, Meola A, Haouz A, et al. PLA2G1B is involved in CD4 anergy and CD4 lymphopenia in HIV-infected patients. The Journal of Clinical Investigation. 2020;130(6):2872-87.
9. Vijayakumar S, Viswanathan S, Aghoram R. Idiopathic CD4 Lymphocytopenia: Current Insights. Immunotargets Ther. 2020;9:79-93.
10. Afinogenova Y, Brooks JP. Idiopathic CD4 Lymphopenia. In: Bernstein JA, editor. Primary and Secondary Immunodeficiency: A Case-Based Guide to Evaluation and Management. Cham: Springer International Publishing; 2021. p. 139-47.
11. Geyer JT. Monocytosis. In: Wang SA, Hasserjian RP, editors. Diagnosis of Blood and Bone Marrow Disorders. Cham: Springer International Publishing; 2018. p. 195-224.
12. Glasser RM, Walker RI, Herion JC. The Significance of Hematologic Abnormalities in Patients With Tuberculosis. Archives of Internal Medicine. 1970;125(4):691-5.
13. Le Voyer T, Neehus A-L, Yang R, Ogishi M, Rosain J, Alroqi F, et al. Inherited deficiency of stress granule ZNFX1 in patients with monocytosis and mycobacterial disease. Proceedings of the National Academy of Sciences. 2021;118(15):e2102804118.

14. Hill RW, Bayrd ED. Phagocytic reticuloendothelial cells in subacute bacterial endocarditis with negative cultures. Annals of internal medicine. 1960;52(2):310-9.
15. Halim N, Ajayi O, Oluwafemi F. Monocytosis in acute malaria infection. Nigerian Journal of Clinical Practice. 2002;5(2):106-8.
16. Newburger PE, Dale DC. Evaluation and Management of Patients With Isolated Neutropenia. Semin Hematol. 2013;50(3):198-206.
17. Hamad H, Mangla A. Lymphocytosis. StatPearls. Treasure Island (FL)2022.
18. Mangaonkar AA, Tande AJ, Bekele DI. Differential Diagnosis and Workup of Monocytosis: A Systematic Approach to a Common Hematologic Finding. Current Hematologic Malignancy Reports. 2021;16(3):267-75.
19. Kratz A, Lee S-h, Zini G, Riedl JA, Hur M, Machin S, et al. Digital morphology analyzers in hematology: ICSH review and recommendations. International Journal of Laboratory Hematology. 2019;41(4):437-47.
20. Roussel M, Davis BH, Fest T, Wood BL, Hematology obotICfSi. Toward a reference method for leukocyte differential counts in blood: Comparison of three flow cytometric candidate methods. Cytometry Part A. 2012;81A(11):973-82.
21. Yamade K, Yamaguchi T, Nagai Y, Kamisako T. Performance evaluation of leukocyte differential on the hematology analyzer Celltac G compared with two hematology analyzers, reference flow cytometry method, and two manual methods. Journal of Clinical Laboratory Analysis. 2021;35(8):e23827.
22. Nassar M, Doan M, Filby A, Wolkenhauer O, Fogg DK, Piasecka J, et al. Label-Free Identification of White Blood Cells Using Machine Learning. Cytometry Part A. 2019;95(8):836-42.
23. Ryu D, Kim J, Lim D, Min H-S, Yoo IY, Cho D, et al. Label-Free White Blood Cell Classification Using Refractive Index Tomography and Deep Learning. BME Frontiers. 2021;2021:9893804.
24. Li W, Wang L, Luo C, Zhu Z, Ji J, Pang L, et al. Characteristic of Five Subpopulation Leukocytes in Single-Cell Levels Based on Partial Principal Component Analysis Coupled with Raman Spectroscopy. Applied Spectroscopy. 2020;74(12):1463-72.
25. Zheng S, Lin JC-H, Kasdan HL, Tai Y-C. Fluorescent labeling, sensing, and differentiation of leukocytes from undiluted whole blood samples. Sensors and Actuators B: Chemical. 2008;132(2):558-67.
26. Shi W, Guo LW, Kasdan H, Fridge A, Tai Y, editors. Leukocyte 5-part differential count using a microfluidic cytometer. 2011 16th International Solid-State Sensors, Actuators and Microsystems Conference; 2011 5-9 June 2011.
27. Shi W, Guo L, Kasdan H, Tai Y-C. Four-part leukocyte differential count based on sheathless microflow cytometer and fluorescent dye assay. Lab on a Chip. 2013;13(7):1257-65.
28. Powless A, Conley R, Freeman K, Muldoon T. Considerations for point-of-care diagnostics: evaluation of acridine orange staining and postprocessing methods for a three-part leukocyte differential test. Journal of Biomedical Optics. 2017;22(3):035001.
29. Bills MV, Nguyen BT, Yoon JY. Simplified White Blood Cell Differential: An Inexpensive, Smartphone- and Paper-Based Blood Cell Count. IEEE Sensors Journal. 2019;19(18):7822-8.
30. McCracken KE, Yoon J-Y. Recent approaches for optical smartphone sensing in resource-limited settings: a brief review. Analytical Methods. 2016;8(36):6591-601.

31. Hassan U, B. Reddy J, Damhorst G, Sonoiki O, Ghonge T, Yang C, et al. A microfluidic biochip for complete blood cell counts at the point-of-care. TECHNOLOGY. 2015;03(04):201-13.
32. Hollis VS, Holloway JA, Harris S, Spencer D, van Berkel C, Morgan H. Comparison of venous and capillary differential leukocyte counts using a standard hematology analyzer and a novel microfluidic impedance cytometer. 2012.
33. Holmes D, Pettigrew D, Reccius CH, Gwyer JD, van Berkel C, Holloway J, et al. Leukocyte analysis and differentiation using high speed microfluidic single cell impedance cytometry. Lab on a Chip. 2009;9(20):2881-9.
34. Liu R, Arifuzzman AKM, Wang N, Civelekoglu O, Sarioglu AF. Electronic Immunoaffinity Assay for Differential Leukocyte Counts. Journal of Microelectromechanical Systems. 2020;29(5):942-7.
35. Hassan U, Watkins NN, Reddy B, Damhorst G, Bashir R. Microfluidic differential immunocapture biochip for specific leukocyte counting. Nature Protocols. 2016;11(4):714-26.
36. Civelekoglu O, Liu R, Usanmaz CF, Chu CH, Boya M, Ozkaya-Ahmadov T, et al. Electronic measurement of cell antigen expression in whole blood. Lab Chip. 2022;22(2):296-312.
37. Civelekoglu O, Wang N, Boya M, Ozkaya-Ahmadov T, Liu R, Sarioglu AF. Electronic profiling of membrane antigen expression via immunomagnetic cell manipulation. Lab Chip. 2019;19(14):2444-55.
38. Shapiro HM. Practical flow cytometry. 4th ed. New York: Wiley-Liss; 2003. l, 681 p. p.
39. Brown M, Wittwer C. Flow cytometry: principles and clinical applications in hematology. Clin Chem. 2000;46(8 Pt 2):1221-9.
40. Givan AL. Principles of flow cytometry: an overview. Methods Cell Biol. 2001;63:19-50.
41. Naeim F. Atlas of hematopathology: morphology, immunophenotype, cytogenetics, and molecular approaches: Academic Press; 2012.
42. McCloskey KE, Chalmers JJ, Zborowski M. Magnetophoretic mobilities correlate to antibody binding capacities. Cytometry. 2000;40(4):307-15.
43. McCloskey KE, Moore LR, Hoyos M, Rodriguez A, Chalmers JJ, Zborowski M. Magnetophoretic cell sorting is a function of antibody binding capacity. Biotechnol Prog. 2003;19(3):899-907.
44. Liu R, Wang N, Kamili F, Sarioglu AF. Microfluidic CODES: a scalable multiplexed electronic sensor for orthogonal detection of particles in microfluidic channels. Lab Chip. 2016;16(8):1350-7.
45. Liu R, Waheed W, Wang N, Civelekoglu O, Boya M, Chu CH, et al. Design and modeling of electrode networks for code-division multiplexed resistive pulse sensing in microfluidic devices. Lab Chip. 2017;17(15):2650-66.
46. Liu R, Wang N, Asmare N, Sarioglu AF. Scaling code-multiplexed electrode networks for distributed Coulter detection in microfluidics. Biosens Bioelectron. 2018;120:30-9.
47. Gold R. Optimal binary sequences for spread spectrum multiplexing (Corresp.). IEEE Transactions on Information Theory. 1967;13(4):619-21.
48. Loos H, Blok-Schut B, Kipp B, van Doorn R, Meerhof L. Size distribution, electronic recognition, and counting of human blood monocytes. Blood. 1976;48(5):743-53.
49. Civelekoglu O, Wang N, Arifuzzman AKM, Boya M, Sarioglu AF. Automated lightless cytometry on a microchip with adaptive immunomagnetic manipulation. Biosensors and Bioelectronics. 2022;203:114014.

1

Table 1: Comparison of the experimental results with independent validation methods for three donors.

		Lymphocytes (%)	Granulocytes (%)	Monocytes (%)
Donor #1	MACY	34.46	54.32	10.22
	Hematology analyzer	34	55.1	10.9
	FC - CD33	34.2	55.0	10.8
	FC - CD45	36.2	53.1	10.7
Donor #2	MACY	27.54	63.24	9.22
	Hematology analyzer	25.9	62.7	11.4
	FC - CD33	29.3	62.1	8.58
	FC - CD45	30.3	61.0	8.7
Donor #3	MACY	36.38	55.32	8.30
	Hematology analyzer	35.1	54.3	10.6
	FC - CD33	35.3	54.4	10.3
	FC - CD45	37.9	51.9	10.2

Table 2: Linear regression analysis of our measurements with respect to the conventional methods and the resulting slope, y-axis intercept, R^2 and root mean square error (RMSE).

	Compared to	Slope	Intercept	R^2	RMSE
Lymphocytes	Hematology analyzer	0.7687	5.775	0.8955	2.9505
	FC - CD33	1.0040	-2.083	0.8334	5.0446
	FC - CD45	1.0140	1.013	0.9237	3.7584
Granulocytes	Hematology analyzer	0.8750	7.487	0.9543	2.3682
	FC - CD33	1.1080	-5.642	0.9578	2.8760
	FC - CD45	1.1830	-11.58	0.9202	4.8412
Monocytes	Hematology analyzer	0.6442	3.606	0.5693	2.4581
	FC - CD33	0.5809	3.380	0.5621	2.2583
	FC - CD45	0.7661	1.706	0.7450	1.9742

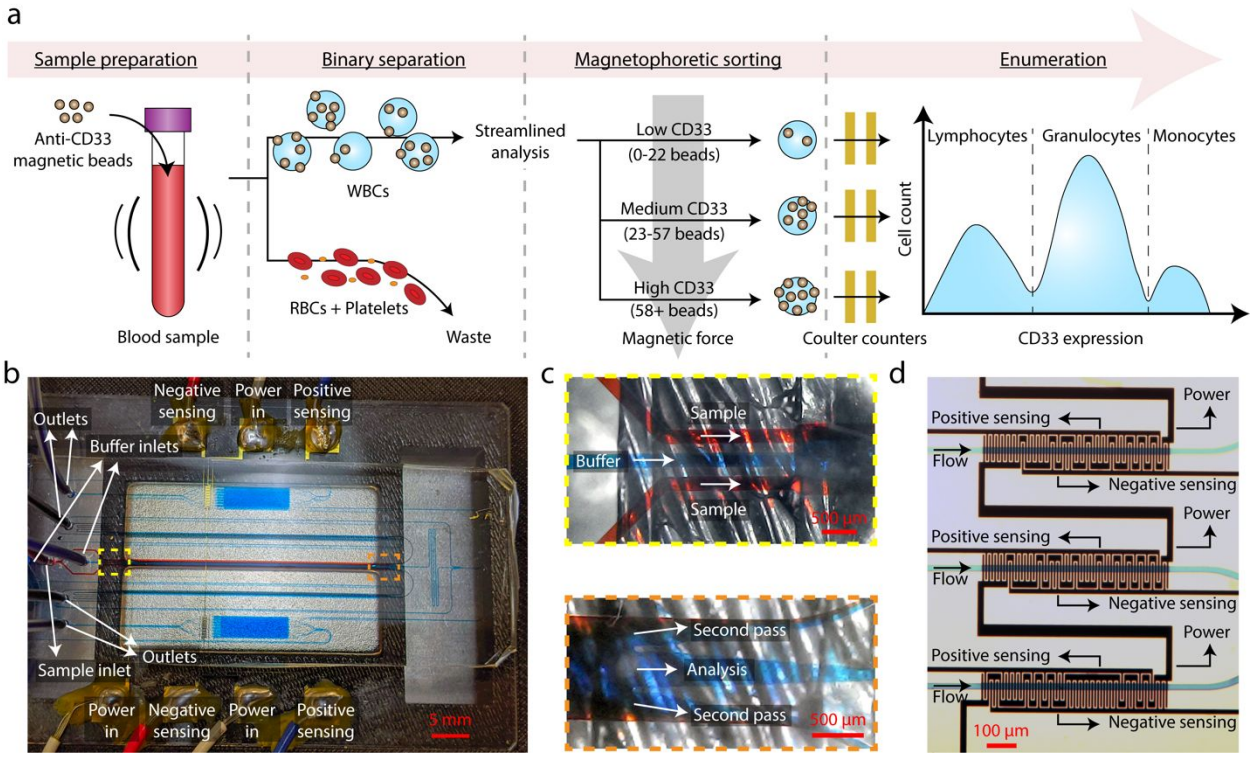

Figure 1: Microchip design and operation. (a) A schematic showing the process flow of assay classifying leukocytes based on their CD33 surface expression. (b) A photo of the microfluidic chip filled with dye solution for visual illustration. The neodymium magnets which provided the magnetic field gradient for cell sorting are also visible beneath the device in a 3D-printed housing. The top layer of the housing that contained two other neodymium magnets required for operation was removed to take this photo. Blue dye was used in place of the buffer solution, while the red dye represented the blood sample. (c) Microscope images of binary sorting channel that eliminated unlabeled blood cells. (d) Microscope images of 3 of the (16 in total across the chip) barcoded electronic sensors. Each sensor produced a distinct 31-bit digital code due to their unique electrode patterns.

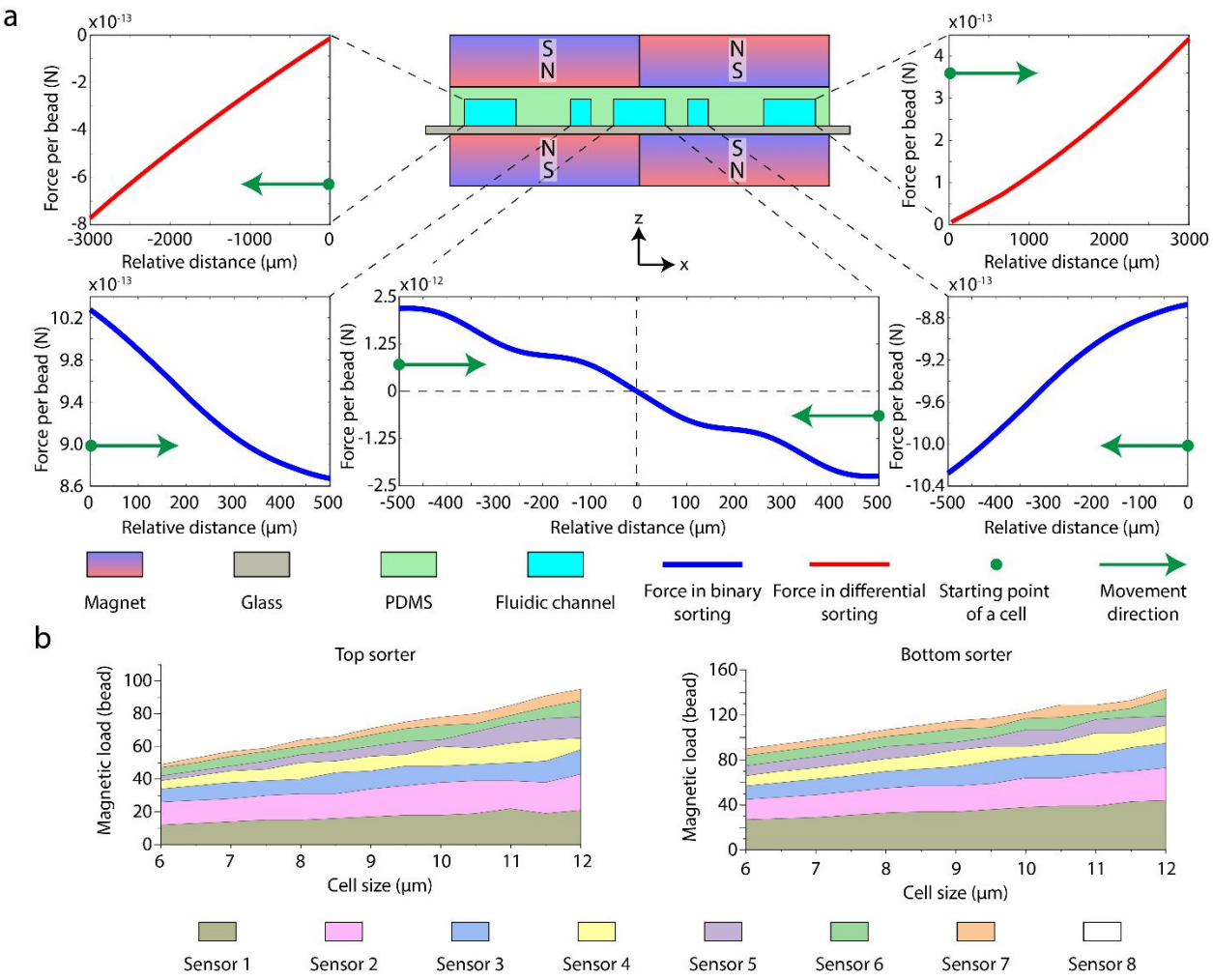

Figure 2: Computational modeling of the immunomagnetic sorting of leukocytes. (a) The cross-sectional schematic shows the placement of the permanent magnets with respect to the microfluidic channels. The plots show the simulated magnetic forces acting on magnetic beads attached to cells in the binary separation (blue lines) and differential sorting (red lines) chambers. Green dots show initial position of a cell while green arrows show the direction of the acting force. (b) Look-up tables for each sensor in the top and bottom differential sorting chambers for a sample flow rate of 1.5 mL/h. The number of magnetic beads on each sorted cell was estimated based on these look-up tables once the raw sensor data was processed to extract sensor identity and cell size.

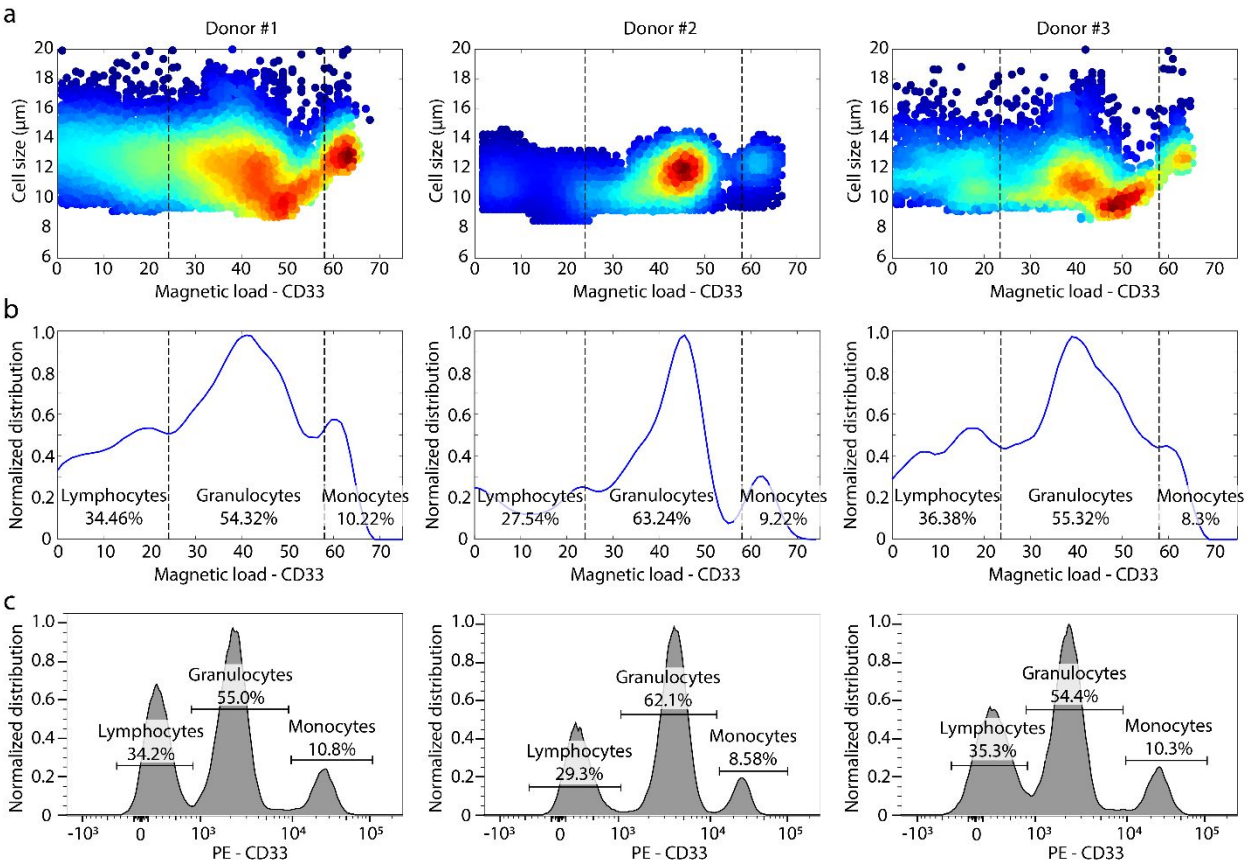

Figure 3: Analysis of healthy blood samples and setting immunomagnetic load gates. (a) Scatter plots of cell size and CD33 immunomagnetic load data obtained for different donor samples. The color gradient shows the density. The two immunomagnetic load gates, one at 23 beads and the other at 58 beads, were used to differentiate lymphocytes, granulocytes, and monocytes and are shown in each plot as dashed lines. (b) Normalized frequencies of the leukocytes based on their CD33 immunomagnetic load. Calculated frequency of different leukocyte subpopulations based on the set gates. (c) Normalized frequencies of leukocytes in matched samples based on flow cytometry measurement of CD33 expression. Frequencies of different leukocyte subpopulations were calculated based on gates on fluorescence intensity.

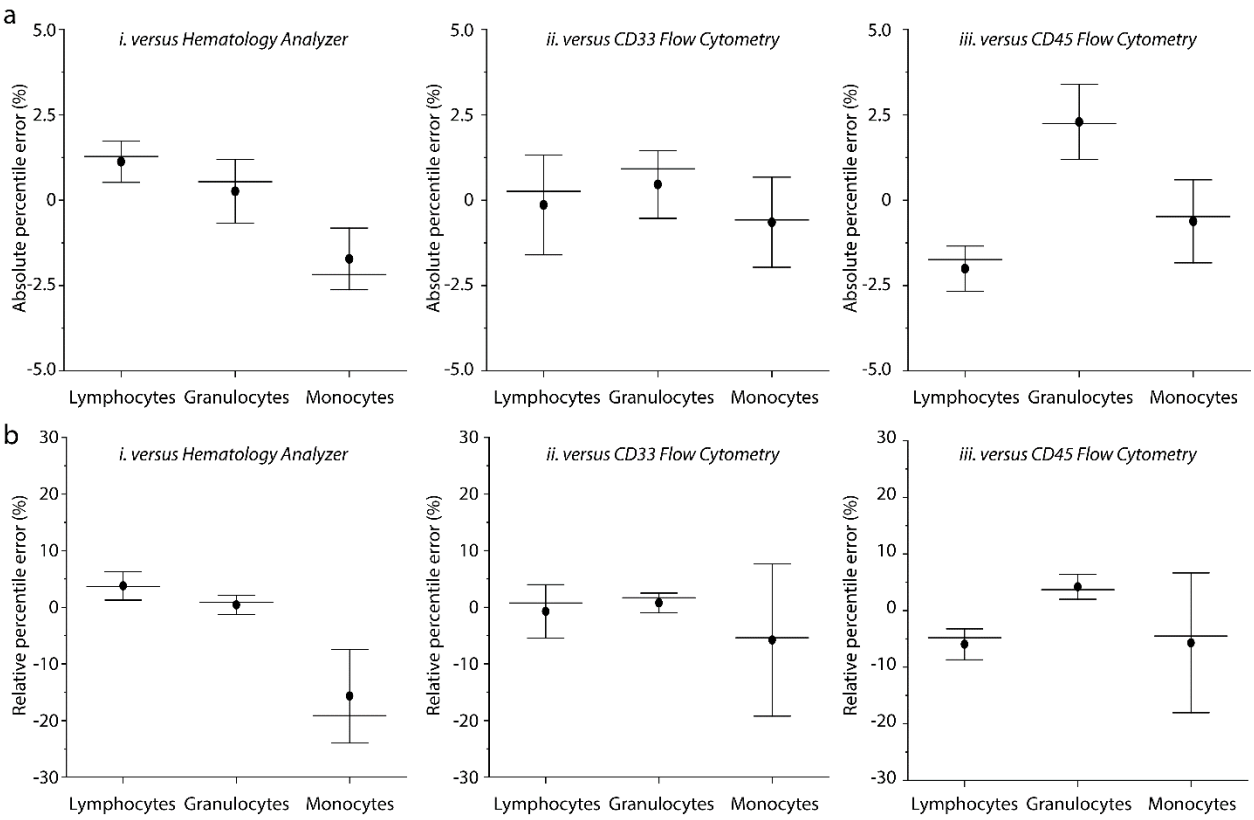

Figure 4: Benchmarking the assay against conventional methods using healthy blood samples. (a) Absolute and (b) relative percentile errors between leukocyte differential data from MACY and the measurements using hematology analyzer (left), fluorescence-based flow cytometry for CD33 (middle) and CD45 (right) expression. In all plots, the dots represent the mean, error bars represent the standard deviation and central line represents the median.

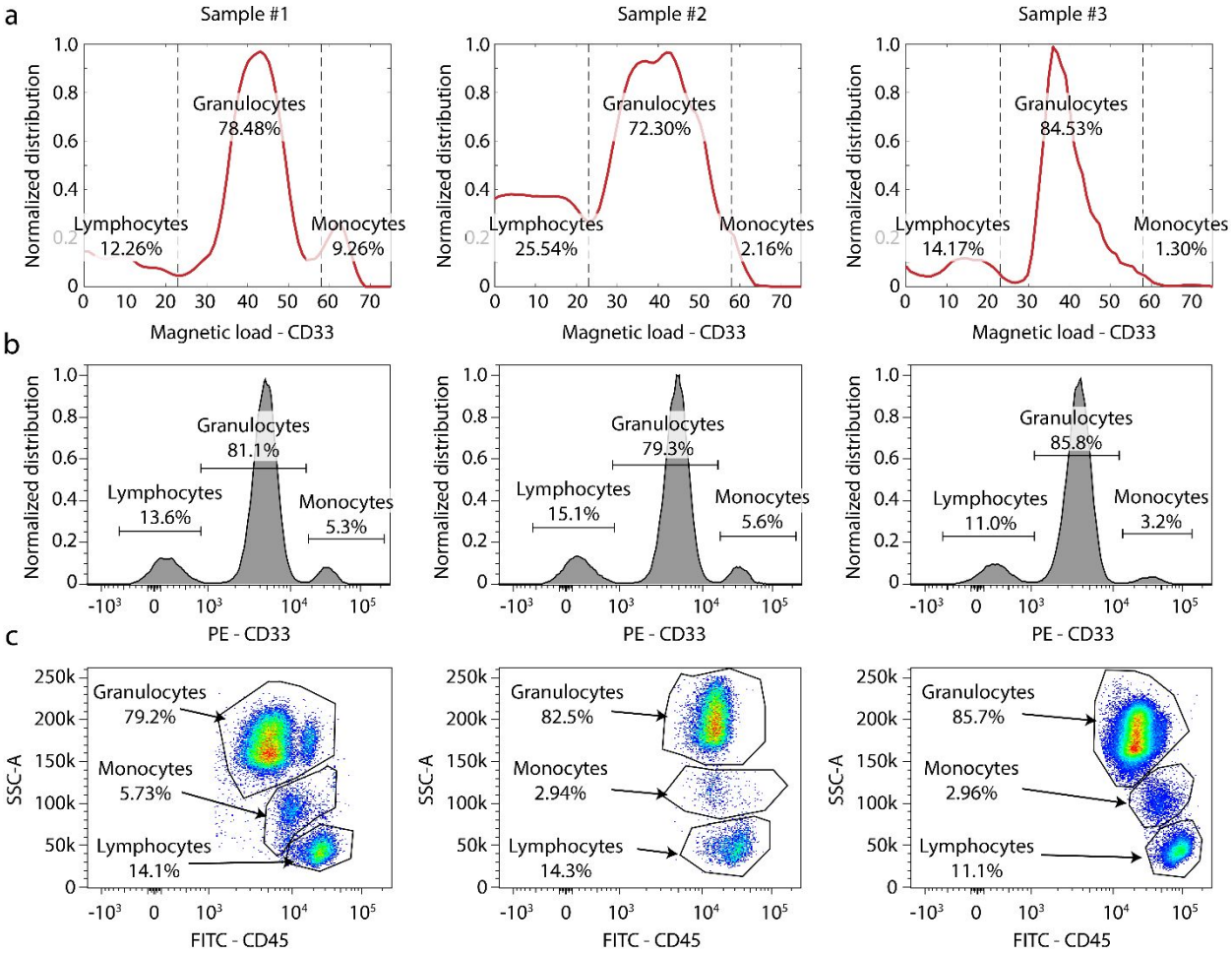

Figure 5: Analysis of blood samples with manipulated leukocyte composition. (a) Measured immunomagnetic load distribution and leukocyte differential results from MACY. (b) Fluorescence flow cytometry measurements of CD33 antigen expression of leukocytes and the leukocyte differential results for matched samples. (c) Scatter plots showing the CD45 expression and the side-scatter for matched samples. Measured leukocyte differential results along with gates for differentiation are shown on the plots.

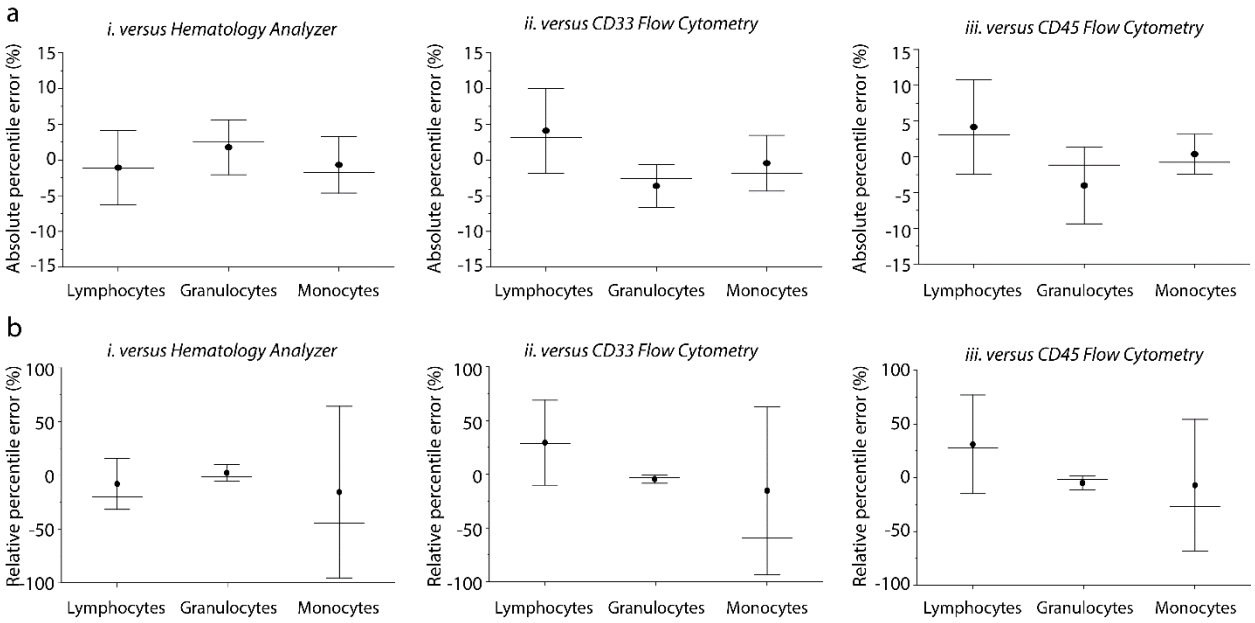

Figure 6: Comparison of the assay results with conventional methods using blood samples with manipulated leukocyte composition. (a) Absolute and (b) relative errors between leukocyte differential data from MACY and the measurements using hematology analyzer (left), fluorescence-based flow cytometry for CD33 expression (middle) and side-scatter analysis combined with CD45 expression (right). In all plots, the dots represent mean, error bars represent standard deviation and central line represents the median.